Commissioning of the Xenoscope Time Projection Chamber for the DARWIN Dark Matter Observatory

Yunjing Wang, Haverford College

Advisors: Prof. Laura Baudis and Dr. Diego Ramírez García, University of Zurich

Abstract

Xenoscope at the University of Zurich is an R&D platform for the DARWIN observatory. It aims to validate electron drift in a 2.6-meter tall TPC and optimize purification rates for DARWIN's goals. After installing the TPC in the Xenoscope cryostat and filling it with about 350 kg of LXe, various subsystems were commissioned. This report focuses on the detector filling, operation, and calibration of the level meter sensors to achieve optimal conditions for dual-phase TPC operation.

1. The Xenoscope facility

The DARWIN (DARk matter WImp search with liquid xenoN) observatory will aim at directly detecting dark matter in the form of weakly interacting massive particles (WIMPs) (Aalbers et al. 2016). It will deploy a target liquid xenon (LXe) mass of about 50 tonnes in a dual-phase time projection chamber (TPC), a technology already in use for the most sensitive WIMP detectors to date (Akerib et al. (2020),Aprile et al. (2024),Zhao & Liu (2018)).

The Xenoscope facility at the University of Zurich, sketched in Figure 1 is part of the rich R&D program towards the realization of DARWIN. Xenoscope is a full-scale vertical demonstrator aiming to address the key electric field and purity requirements for drifting electrons over a 2.6 m TPC(Girard 2023). Its core consists of a small-diameter cryostat of the entire planned DARWIN height, able to host about 400 kg of LXe. The cryogenic, gas purification and storage systems complete the assembly and ensure that the Xe is safely stored and, when in use, constantly kept cold and purified.

After successfully commissioning the facility (Baudis et al. 2021) and operating a purity monitor in LXe (Baudis et al. 2023), a TPC was recently installed inside the Xenoscope cryostat. Schumann (2014) discusses the dual-phase LXe TPC's principles and dark matter physics potential. This report covers contributions to the Xenoscope TPC's commissioning, including LXe filling monitoring, and the operation and calibration of level meters and the weir, which ensure the liquid-gas interface is correctly positioned. Section 2 details the TPC components, while sections 3 and 4 focus on detector filling and LXe leveling, respectively. Concluding remarks are in section 5.

2. The dual-phase Xenoscope TPC

Figure 2 shows the P&ID of the Xenoscope facility, which highlights both the xenon filling paths (red and blue) and the recirculation path where the xenon gets purified (purple). During the filling and recuperation process, capacitive levelmeters provide continuous readout of the liquid level. Controlling the liquid-gas interface position and potential tilt is crucial, as it must be stably centered between the gate and anode electrodes for optimal electron extraction and proportional scintillation signal generation, as described in Schumann (2014).

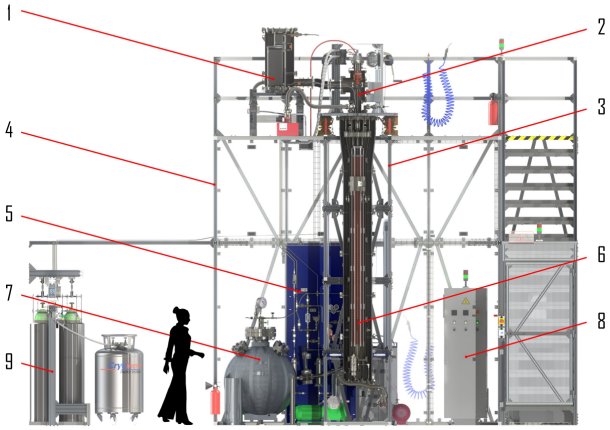

Fig. 1.—: Render of the Xenoscope facility, with the 2.6-meter TPC mounted in a 24.8-cm-diameter cryostat. Legend: (1) Heat exchanger; (2) Cooling tower; (3, 4) Structure frames, (5) Purification gas panel; (6) TPC in the cryostat; (7) High-pressure liquid recovery xenon storage; (8) Power distribution cabinet; (9) Gas cylinder storage Array. Figure adapted from Baudis et al. (2021).

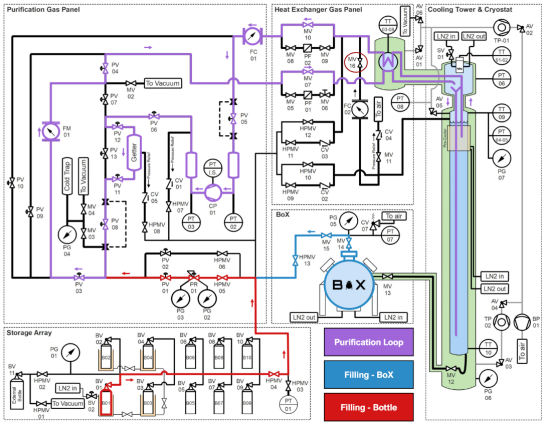

Fig. 2.—: P&ID of the filling procedure. High-pressure GXe is taken from the bottle array (red path) or BoX (blue path). The pressure regulator (PR-01) is used to add GXe to the recirculation loop (purple path). The difference in flow between the flow controller (FC-01) and the flow meter (FM-01) is used as a metric of the added xenon. Figure adapted from Girard (2023)

2.1. Levelmeters

The TPC uses long levelmeters (LLMs) and short levelmeters (SLMs). Their working principle relies on the dependence of the capacitance C with the dielectric materials between the electrodes. In this case the capacitance C relies on the LXe level:

$$C = \frac{Q}{U} = \frac{\oint_A D \cdot dA}{\int_s E \cdot ds} = \epsilon_0 \epsilon_r \cdot \frac{\oint_A E \cdot dA}{\int_s E \cdot ds}, \tag{1}$$

where Q is the charge, U is the potential difference, D is the electric displacement field, E is the electric field, ϵ_0 is the permittivity of free space, ϵ_r is the relative permittivity of the dielectric material, LXe in this case,dA represents an infinitesimal element of the area A over which the electric displacement field D or electric field E is integrated, while ds represents an infinitesimal element of the path s along which the electric field E is integrated. For the same relative permittivity ϵ_0 form the same material, the distance between the cathode and anode D, in this case, the liquid level, determines the capacitance, as the cross section A and electric potential U never changes. To be more specific, there is a linear relationship between the potential and the distance. Therefore, the capacitance can be used to measure the height of LXe in the TPC.

Long Levelmeters

The LLM system covers the entire length of the TPC, from the bottom to above the anode, enabling continuous data collection during LXe filling and recuperation. The LLM is divided into two overlapping segments, referred to as the upper and lower LLMs.

The capacitance of a LLM segment ranges from $C_{min} = 130.2$ pF in GXe to $C_{max} = 251.3$ pF when fully immersed in LXe. Spacers at known heights on the LMs serve as calibration rings, allowing to establish the practical relationship between capacitance and height.

Short levelmeters

The SLM system consists of three 30 mm-long LMs, symmetrically arranged around gate and anode. The SLM can detect if the TPC is tilted. Contact with the LXe surface causes an initial capillary rise, used for calibration, with a predicted height of 4.5 mm.

The SLMs have a cylindrical geometry with a dynamic capacitance range of $\Delta C/h = 0.45$ pF/mm. The capacitance changes from $C_{min} = 14.2$ pF in GXe to $C_{max} = 27.8$ pF when submerged in LXe.

2.2. Weir

The weir, located at the top of the TPC, is an open vessel designed to fine-tune the liquid height, ensuring it stays between the anode and gate at the end of the filling process. The weir, schematically shown in Figure 3, controls the LXe level by allowing liquid to leak into the overspill cylinder and be extracted through the pipe once it reaches the leak point. However, if the weir is fully submerged and the extraction pipe cannot remove the liquid quickly enough, the weir is unable to effectively act on the LXe level.

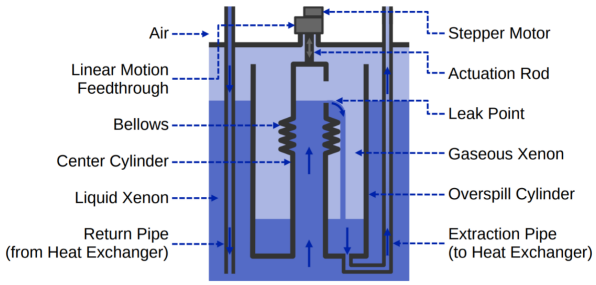

Fig. 3.—: Schematic diagram of the weir. Figure adapted from Bismark, 2024, unpublished PhD dissertation.

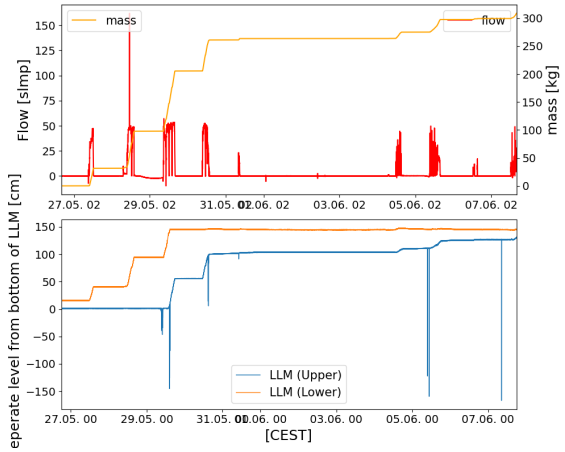

Fig. 4.—: (Top) LXe mass calculated by integrating the flow with LLM readouts. The upper plot shows the new flow (red) and mass estimate (orange). The lower plot displays the LLM levels from capacitance readings.

2.3. Gas purification path

As shown in Figure 2, MV-16 is a valve in the purification loop that controls whether gas from the TPC is extracted into the heat exchanger: when MV-16 is open, both LXe and GXe are extracted; when closed, only liquid is extracted. This new design, implemented after the first operation Baudis et al. (2021), aims to purify GXe to prevent electron absorption by contaminants in the gas. During the SLM system calibration and monitoring, the impact of operating this valve must be assessed,

as it may act directly on the level of the gas-liquid interface.

3. Liquid xenon transfer to the cryostat

For the initial operation phase (April 23 to June 20), the TPC was filled with xenon from the gas bottle array (red path in Figure 2, while being liquified and recirculated (purple path in Figure 2). The mass introduced to the system was monitored via the difference in the readings from the flow meters FC-01 (recirculation) and FM-01 (recirculation + xenon input).

By integrating the flow readings over time, in units of standard liters per minute (slpm), we converted the flow data into mass, which allowed us to compare xenon mass with the capacitance readings of the long and short leveleters. The synchronous rise of capacitance and mass, as shown in Figure 4, indicates a good match between the data sets.

Calibration of the LLMs was done by identifying the positions of calibration rings on the lower and upper LLM segments. Each segment has five evenly spaced calibration rings, each 3 cm long. These rings create small plateaus in the capacitance readings during filling. The approximate calibration function used was $C = 130.2$ pF$+0.743$ pF/cm$\cdot(n \cdot 24$ cm), where C is the capacitance and n is the calibration ring number. The data collected are shown in Tables 1 and 2, with linear fits yielding rate of change of capacitance per unit length of 0.748 for the upper LLM and 0.745 for the lower LLM.

Height (cm)	Capacitance (pF)
24	148.55 ±0.05
48	166.60 ±0.05
72	184.45 ±0.05

Table 1:: Upper LLM Data

Height (cm)	Capacitance (pF)
24	148.35 ±0.05
48	166.10 ±0.05
72	184.10 ±0.05
86	201.95 ±0.05
120	219.80 ±0.05

Table 2:: Lower LLM Data

SLM	C_{min}	C_{cap}	C_{max}
SLM1	13.8 ±0.01	15.4 ±0.07	25.0 ±0.01
SLM2	14.0 ±0.01	15.6 ±0.07	25.4 ±0.01
SLM3	14.0 ±0.01	15.5 ±0.07	25.4 ±0.01

Table 3:: SLM Data

4. Liquid xenon leveling

In the final phase of the filling operation, the main focus was to stably set the LXe level in between the gate and anode via the weir, MV-16 and the more precise SLMs.

4.1. SLMs Calibration

Plateaus observed in the data, as shown in the figure, are used to calculate the average values. Results are summarized in the Table 3 . The general form of the the height-capacitance relationship is

$$h = (C - C_{cap})/(C_{max} - C_{min})3cm\,, \tag{2}$$

where C_{cap} is the capacitance just after the capillary rise. Derived by the general form, the final calibration function of the thred SLMs are:

- SLM 1 Fit line: $h[cm] = 0.26780 \cdot C[pF] - 4.13281$
- SLM 2 Fit line: $h[cm] = 0.26375 \cdot C[pF] - 4.11449$
- SLM 3 Fit line: $h[cm] = 0.26289 \cdot C[pF] - 4.07798$

4.2. Weir operation

The operation of the weir during running conditions is shown in in Figure 5. When the weir is lowered by 2 mm, as shown in step 5, the liquid level also drops by 2 mm. However, as steps 8 and 9 demonstrate, once the weir is fully submerged, further changes to the weir do not affect the liquid level.

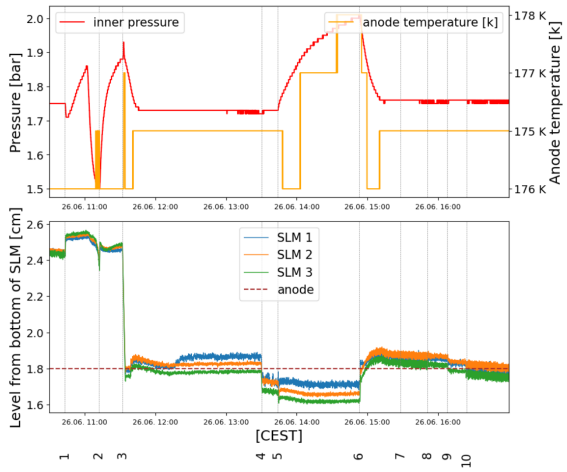

Fig. 5.—: Pressure, temperature and LXe SLMs readings in the TPC. Key steps: (5) Weir lowered by 2 mm, (8) Weir lowered by 2 mm, (9) Weir raised by 4 mm, (11) Weir lowered by 2 mm

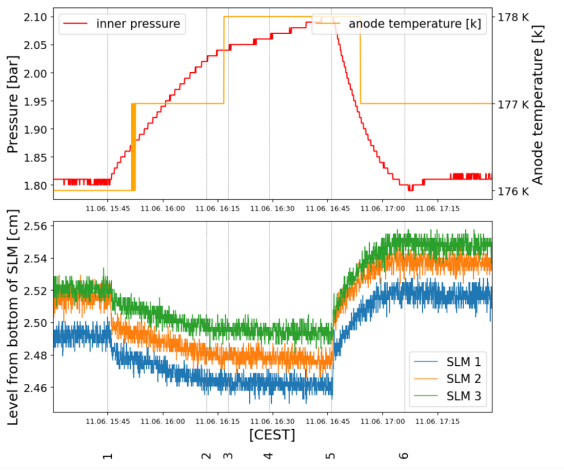

Fig. 6.—: Pressure, temperature and LXe SLMs readings in the TPC. Key steps: (1) Extracting liquid (MV-16 closed), (5) Extracting gas and liquid (MV-16 open).

4.3. MV-16 operation

It was observed that when opening MV-16 the extraction of gas phase was be much faster than the extraction of liquid phase, which caused a reduction in pressure and avraise the LXe level. The increase in pressure would also cause the capacitance to rise for the SLMs.

Figure 6 shows as an example of this observation: by reducing the setpoint temperature of the system, the pressure decreased, which caused a lower rate of dropping for the LXe level. Opening MV-16 reduced the pressure, so that the LXe level rise quickly.

In the final stage, the tuning of LXe level request a stable pressure, as the valve operation varies the pressureMV-16 should be closed.

5. Conclusions

The Xenoscope facility is instrumental to benchmark the technologies necessary for the DARWIN project, particularly through the successful operation of its 2.6-m TPC.

This report focuses on assessing the reliability of the capacitive levelmeters and the leveling systems. By means of the operations here described, the entire filling of the detector (~350 kg of LXe) was pursued, along with the calibration of the leveling system and the successful leveling of the liquid-gas interface between the gate and the anode. This last operation ensured dual-phase

TPC operation and enabled the commissioning of the Xenoscope TPC.

Acknowledgments: We gratefully acknowledge support from Thinkswiss scholarship and KNISC funding.

References

Aalbers J., et al., 2016, arXiv preprint arXiv:1606.07001

Akerib D., et al., 2020, Nuclear Instruments and Methods in Physics Research Section A: Accelerators, Spectrometers, Detectors and Associated Equipment, 953, 163047

Aprile E., et al., 2024, The European Physical Journal C, 84

Baudis L., et al., 2021, Journal of Instrumentation, 16, P08052

Baudis L., et al., 2023, European Physical Journal C, 83

Girard F., 2023, Dissertation, dr. sc. nat., University of Zurich, Zurich, Switzerland, doi:https://www.physik.uzh.ch/dam/jcr:1a7e7134-bf33-4c98-ad13-ca6d863b9f2b/F˙Girard˙PhD˙Thesis.pdf

Schumann M., 2014, Journal of Instrumentation, 9, C08004–C08004

Zhao L., Liu J., 2018, Modern Physics Letters A, 33, 1830013